A&A 459, 843–847 (2006)
DOI: 10.1051/0004-6361:20065990

Astronomy & Astrophysics

X-ray and He I 1.0830 μm emission from protostellar jets *(Research Note)*

R. Liseau

Stockholm Observatory, AlbaNova University Center, 106 91 Stockholm, Sweden
e-mail: rene@astro.su.se

Received 7 July 2006 / Accepted 31 August 2006

ABSTRACT

Context. The high energies of protostellar jets, implied by recent observations of X-rays from such flows, came very much as a surprise. Inferred shock velocities are considerably higher than what was previously known, hence putting even larger energy demands on the driving sources of the jets. The statistics of X-ray emitting jets are still poor, yet a few cases exist which seem to imply a correlation between the presence of He I 1.0830 μm emission and X-ray radiation in a given source.
Aims. This tentative correlation needs confirmation and explanation. If the jet regions of He I 1.0830 μm emission are closely associated with those producing X-rays, high resolution infrared spectroscopy can be used to observationally study the velocity fields in the hot plasma regions of the jets. This would provide the necessary evidence to test and further develop theoretical models of intermediately fast (>500−1500 km s^{-1}) interstellar shock waves.
Methods. The HH 154 jet flow from the embedded protostellar binary L 1551 IRS 5 provides a case study, since adequate IR and X-ray spectroscopic data are in existence. The thermal X-ray spectrum is fed into a photoionization code to compute, in particular, the line emission of He I and H I and to account for the observed unusual line intensity ratios.
Results. The advanced model is capable of accounting for most observables, but shows also major weaknesses. It seems not unlikely that these could, in principle, be overcome by a time dependent hydrodynamical calculation with self-consistent cooling. However, such sophisticated model development is decisively beyond the scope of the present work.
Conclusions. Continued X-ray observations, coordinated with simultaneous high resolution infrared spectroscopy, are highly desirable.

Key words. ISM: Herbig-Haro objects – ISM: jets and outflows – ISM: individual objects: L 1551 IRS 5 – stars: formation – stars: pre-main sequence

1. Introduction

The radiation from HH-objects and collimated jet flows is a manifestation of interstellar shock waves, the typical velocities of which were believed to be $V_s \ll 500$ km s^{-1} (e.g., Hartigan et al. 1987; Raga et al. 1996; Reipurth & Bally 2001). Unexpectedly, a number of such objects from embedded protostars have recently been detected at X-ray energies (Pravdo et al. 2001; Favata et al. 2002; Preibisch 2003; Pravdo et al. 2004; Tsujimoto et al. 2004; Güdel et al. 2005; Grosso et al. 2006, with reference to HH 1/2, HH 154, Ser SMM1, HH 80/81, TKH 8, HH 158, HH 210, respectively).

The X-ray spectra have typically a thermal spectral distribution, characteristic of temperatures of several million degrees. This was very surprising, since implied shock velocities ($\gg$300 km s^{-1}) would be very much higher than what had previously been inferred from spectroscopic observations at longer wavelengths. This indicated that highly significant jet material had escaped detection. As a consequence, there is a potential risk that energy requirements on the jet source, being proportional to the square of the jet velocity, had been seriously underestimated. Proposed energy extraction mechanisms from the protostar-disk system might need to be revised in the light of these new findings.

As in active stars, the *continuous* X-ray emission may be accompanied by He I 1.0830 μm *line* radiation (e.g., Zirin 1982). If that is the case, this line would be a valuable tool to probe the velocity fields of the hottest plasma regions in the jet. Also, in the infrared, extinction problems would be considerably reduced compared to shorter wavelengths and, for consistency checks, recombination lines from hydrogen, i.e. Pβ 1.2818 μm and Pγ 1.0938 μm, could also be observed simultaneously in the photometric J-band.

In Table 1, observations of He I 1.0830 μm and X-rays toward various flows have been compiled. Evidently, many objects lack the He I 1.0830 μm line, but reveal a rich H_2 spectrum, which is consistent with non-dissociative shocks of low velocity, of the order of 10 km s^{-1}. This is true also for HH 1G and the Ser SMM1 jet, toward which both He I 1.0830 μm and X-ray observations have been performed, but neither of which was detected. HH 2H was detected in X-rays but has apparently not been observed spectroscopically in the 1 μm region. On the other hand, the jet flows HH 158 (DG Tau A) and HH 154 (L 1551 IRS 5) were clearly detected in both He I 1.0830 μm and at X-ray wavelengths, lending support to the above proposition.

It is thus the primary objective of this *Research Note* to stimulate further X-ray observations for the investigation of the high energy regions in protostellar jets, alongside with coordinated high resolution near infrared spectroscopy to determine Doppler velocities and line shapes. These data can then be compared with predictions from theoretical shock models.

To date, the best available data are those of the HH 154 flow and we shall first examine the accumulated evidence for this

Table 1. Protostellar jets with X-ray data and/or NIR spectra.

Jet flow	He I 1.0830 μm	X-rays	Reference	Comment
HH 158	×	×	1, 2	[Fe II]
HH 154	×	×	3, 4, 5	[Fe II]
HH 210		×	6	
HH 1G	−×	−×	7, 8	H_2 + [Fe II]
HH 2H		×	8	
TKH 8		×	9	
HH 43	−×		10	H_2
HH 24A	−×		11	H_2 + [Fe II]
HH 25	−×		11	H_2
HH 26	−×		11	H_2
HH 72	−×		11	H_2
Vel IRS17	−×		12	H_2
HH 320	−×		11	H_2
HH 321	−×		11	H_2
HH 80		×	13	
HH 81		×	13	
Ser SMM1	−×	−×	14, 15	H_2
HH 99-B0	×		16	H_2 + [Fe II]

Notes to the table: × = detected, −× means observed but not detected. H_2 indicates the presence of ro-vibrationally excited H_2 lines; [Fe II] the presence of [Fe II] lines; H_2 + [Fe II] the presence of both species along the same line of sight/inside spectrograph slit. When possible, HH-nomenclature follows that of Reipurth (1999).
References: (1) Takami et al. (2002); (2) Güdel et al. (2005); (3) Itoh et al. (2000); (4) Liseau et al. (2005); (5) Favata et al. (2002); (6) Grosso et al. (2006); (7) Nisini et al. (2005); (8) Pravdo et al. (2001); (9) Tsujimoto et al. (2004); (10) Giannini et al. (2002); (11) Giannini et al. (2004); (12) Giannini et al. (2005); (13) Pravdo et al. (2004); (14) Liseau (unpublished); (15) Preibisch (2003); (16) McCoey et al. (2004).

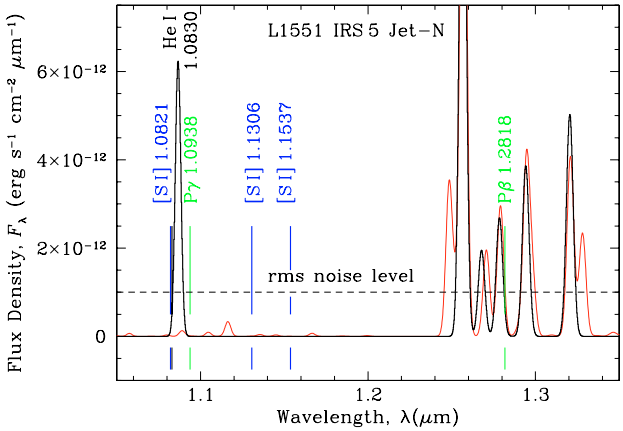

Fig. 1. The J-band spectrum of Itoh et al. (2000) containing the Paschen lines, with the estimated level of the rms noise indicated. The observations are displayed as the black histogram, whereas the smooth red line refers to the fit of the [Fe II] spectrum (for A_V = 5.7 mag, Liseau et al. 2005). The wavelength positions of the recombination lines He I 1.0830 μm, Pγ 1.0938 μm and Pβ 1.2818 μm are indicated above and below the spectrum. This applies also to the wavelengths of the transitions to the inverted ground state of [S I], i.e. $^1D_2$–$^3P_2$ 1.08212 μm, $^1D_2$–$^3P_1$ 1.13058 μm and $^1D_2$–$^3P_0$ at 1.15376 μm, respectively.

object (Sect. 2). Some numerical model calculations will be presented and discussed in Sect. 3. In that section, we will also conclude with some suggestions for future work.

2. L 1551 jet (HH 154): the data

2.1. Infrared spectroscopy

The examined data are based on the J- and H-band spectroscopy by Itoh et al. (2000). Forbidden lines of ionized iron, [Fe II], dominate the observed spectrum and this has been analysed in depth by Liseau et al. (2005). The spectral resolution near λ = 1.0 μm is quite modest, $\Delta\lambda = 3.6 \times 10^{-3}$ μm (R = 280, ΔV = 10^3 km s^{-1}), which also corresponds to the accuracy with which wavelengths can be read off Fig. 5 in the paper by Itoh et al. (2000).

In Table 2, the line fluxes are given and in Fig. 1, the jet-spectrum between 1.05 μm and 1.35 μm is displayed. Included is the best fit for the [Fe II] transitions of Liseau et al. (2005), shown by the smooth red line, whereas the observations are shown as black histograms (see also Table 2). Liseau et al. (2005) tentatively identified the feature near 1.08 μm as He I $^3P^o_2$–$^3S_1$ 1.083034 μm, and in the following, possible other identifications, because of wavelength overlaps within the errors, are briefly discussed.

2.1.1. [Fe II] 1.0890 μm

A little red "bump" is visible under the observed line near 1.08 μm. This bump is due to [Fe II] a ^{4}H – b ^{2}G at 1.08899 μm, with upper level energy E_{up}/k > 44 000 K. The matching of the observed line with this transition would require, therefore, a much higher level of excitation than what has been inferred from the other lines in the spectrum, and is therefore inconsistent with the observations. Consequently, [Fe II] 1.0890 μm is disregarded as a viable candidate for the 1.08 μm feature.

2.1.2. [S I] 1.0821 μm

Around 1.08 μm, atomic/ionic *ground state* transitions exist only for neutral sulphur. Relatively close in wavelength to the observed feature is [S I] $^1D_2$–$^3P_2$ at 1.082117 μm. The other two transitions to the inverted ground state of sulphur are also in the J-band, viz. $^1D_2$–$^3P_1$ at 1.130585 μm and $^1D_2$–$^3P_0$ at 1.1537564 μm (Fig. 1). None of these latter lines are detected. This is hardly surprising, as sulphur is fully ionized in the jet ($\chi_{S\,I}$ = 10.36 eV), which is further supported by the non-detection of the [S I] 25.25 μm fine structure $^3P_1$–$^3P_2$ line (White et al. 2000). The observed line near 1.08 μm is therefore not due to neutral sulphur.

2.1.3. Pγ 1.0938 μm

Strong Balmer line emission has frequently been observed from the jet (Fridlund et al. 2005, and references therein) and, in view of the high extinction, Paschen lines could be expected to be detectable in the J-band. For instance, using the extinction curve of Rieke & Lebofsky (1985) for the value of A_V = 5.7 mag (derived from the [Fe II] spectrum), the attenuation ("reddening") of the Hα flux corresponds to a factor of 70. In contrast, at the wavelength of Pβ, this extinction amounts to a diminishing factor of only 4. However, based on Hα observations of the jet, the 2.5σ feature at 1.2785 μm would appear to be too strong (if real) by a factor of about 3 to be consistent with Pβ 1.2818 μm. As is evident from Fig. 1, this feature is instead well fit by an [Fe II] line.

For a wide range in density, intrinsic Case B line ratios are typically Pβ/Pγ ~ 2 (Hummer & Storey 1987). Since the observed flux ratio $F(1.2785)/F(1.0866) \ll 1$, and any extinction

Table 2. Wavelength and flux estimates in the *J*- and *H*-band spectra of HH 154 (based on observations by Itoh et al. 2000).

$\lambda^{\dagger}_{\rm obs}$ (μm)	$10^{15} \times F^{\ddagger}_{\rm line}$ (erg cm^{-2} s^{-1})	Identification & $\lambda_{\rm air}$ (μm) (FeII: Quinet et al. 1996)
1.0866	26.0 ± 4.6	He I 1.083034 ^{3}P° 2p–^{3}S 2s
1.2566	70.2 ± 4.6	[Fe II] 1.256680 a^{4}D–a^{6}D
1.2785	13.2 ± 5.2	[Fe II] 1.278776 a^{4}D–a^{6}D
1.2942	19.2 ± 1.6	[Fe II] 1.294268 a^{4}D–a^{6}D
1.3205	25.5 ± 2.1	[Fe II] 1.320554 a^{4}D–a^{6}D
1.3272	19.9 ± 4.0	[Fe II] 1.327776 a^{4}D–a^{6}D
1.5334	20.7 ± 1.1	[Fe II] 1.533471 a^{4}D–a^{4}F
1.5995	13.0 ± 1.7	[Fe II] 1.599473 a^{4}D–a^{4}F
1.6435	112.3 ± 1.9	[Fe II] 1.643550 a^{4}D–a^{4}F
1.6678	8.6 ± 2.0	[Fe II] 1.663766 a^{4}D–a^{4}F
1.6769	13.7 ± 1.7	[Fe II] 1.676876 a^{4}D–a^{4}F
1.7045	5.0 ± 2.0	–
1.7156	6.0 ± 2.0	[Fe II] 1.711129 a^{4}D–a^{4}F
1.7490	6.0 ± 2.0	[Fe II] 1.744934 a^{4}D–a^{4}F
1.8045	13.0 ± 4.0	[Fe II] 1.800016 a^{4}D–a^{4}F
1.8134	22.0 ± 6.6	[Fe II] 1.809395 a^{4}D–a^{4}F
1.0938	1.4 ± 4.6	H I Pγ
1.2818	4.1 ± 5.2	H I Pβ

Notes to the Table: † Estimated accuracy is $\Delta\lambda = \pm 0.004$ μm. ‡ Flux calibration from Y. Itoh (private communication).

correction could only decrease this value even further, the observed feature near 1.08 μm is not due to Pγ.

2.1.4. He I 1.0830

For reasons which will become apparent below, we find that He I 1.0830 μm is the best identification for the observed 1.08 μm feature.

Successful models of the infrared [Fe II] spectrum of the jet implied $A_{\rm V} = 5.7$ mag, where an extinction law of the form $A_\lambda/A_{\rm V} = 3.0134 - 5.621\lambda + 4.3847\lambda^2 - 1.5839\lambda^3 + 0.2181\lambda^4$, $0.55 \leq \lambda \leq 2.2$ μm had been adopted (Rieke & Lebofsky 1985). When the extinction is spectroscopically determined, the uncertainty in $A_{\rm V}$ is often dominated not by the measurement errors, but by the uncertainty in the atomic parameters for the transitions from common upper levels (Table 2; and Fig. 1 of Liseau et al. 2005). For instance, the widely exploited line ratio $F(1.64\ \mu{\rm m})/F(1.25\ \mu{\rm m})$ is not better determined than to the range 0.74–0.96 (Quinet et al. 1996), where the higher value is based on more recent calculations, and which was the preferred one by Liseau et al. (2005). For the observed ratio, extinction estimates would then fall into the range $A_{\rm V} = 5.7$–8.6 mag (subject to the assumed extinction curve).

The extinction corrected luminosity of the He I 1.0830 μm line is $L_{1.0830\ \mu{\rm m}} = 6 \times 10^{28}$ erg s^{-1} ($D = 140$ pc and assuming isotropic emission). This corresponds to 20% of the X-ray luminosity from this region in the jet (see next section).

2.2. X-rays from the 0.3–7.9 keV band

At the distance of 140 pc, the X-ray luminosity is $(2–5) \times 10^{29}$ erg s^{-1} (Favata et al. 2002; Bonito et al. 2004). As can be seen in Fig. 2, these XMM-Newton data are consistent with a thermal source at temperatures of roughly 4×10^6 K. Favata et al. (2002) give the emission measure of the hot gas as $EM = \int (x_{\rm e}\, n_{\rm H})^2\, {\rm d}V = 1.1 \times 10^{52}$ cm^{-3}, yielding an estimate of the source size, the linear scale of which corresponds to a few $\times 10$ AU for densities of the order of 10^4 cm^{-3}.

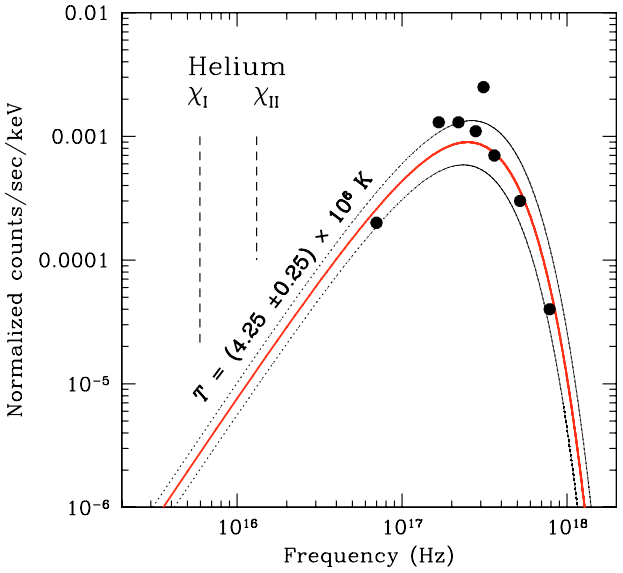

Fig. 2. The observed X-ray spectrum of the L 1551 IRS 5 jet is shown by the big dots, omitting error bars for clarity. The data are limited to roughly 0.3–3.3 keV. The spectrum appears thermal and is consistent with temperatures of about 4–4.5 MK (including observational errors, the best fit MEKAL model yields 4 ± 2.5 MK, Favata et al. 2002). For the model computations, the spectral shape of the blackbody, shown by the continuous curves, has been used as input spectrum (see the text). The frequencies corresponding to the ionization edges of He I and He II are shown by the vertical dashed lines.

A large body of observational data exists for the X-ray spot within the (northern) jet (Fridlund et al. 2005; Liseau et al. 2005). The value of the X-ray attenuation, $A_{\rm V} = (7.3 \pm 2.1)$ mag, is consistent with the visual extinction derived from the infrared [Fe II] spectrum. Conforming with this steep extinction gradient is also the observed Hα/Hβ-ratio (Fridlund et al. 2005).

The analysis of the X-ray data for protostellar jets (Table 1) has generally been in terms of shock waves and has, as such, frequently exploited analytical formulations for the temperature and pre-shock density, with the shock velocity as a parameter (e.g., Ostriker & McKee 1988; Raga et al. 2002). Common results can be summarized as $T > 10^6$ K, $V_{\rm s} > 300$ km s^{-1} and $n_0 \sim$ a few $\times\, 10^2$ cm^{-3} (see the references in Sect. 1).

3. Discussion and conclusion

The overall observational evidence supports the view that the X-ray emission originates from fast shocks in the HH 154 jet, with velocities in excess of 500 km s^{-1} (Favata et al. 2002; Bonito et al. 2004; Liseau et al. 2005; Favata et al. 2006). A reasonable scenario features a hypersonic jet, ramming into molecular cloud material which leads to the complete destruction of molecules and grains and the ionization of the gas, which is heated to high temperatures. This hot plasma is radiatively cooled by X-rays, which are capable of ionizing the neutral gas ahead of the shock, altering its state of excitation and potentially also its chemistry. In order to arrive at quantitative estimates of the associated helium and hydrogen recombination line emission, in particular, we have run photoionization models for this scenario.

The He I 1.0830 μm line originates from levels which are more than 20 eV above the ground (Fig. 3). Evidently, the

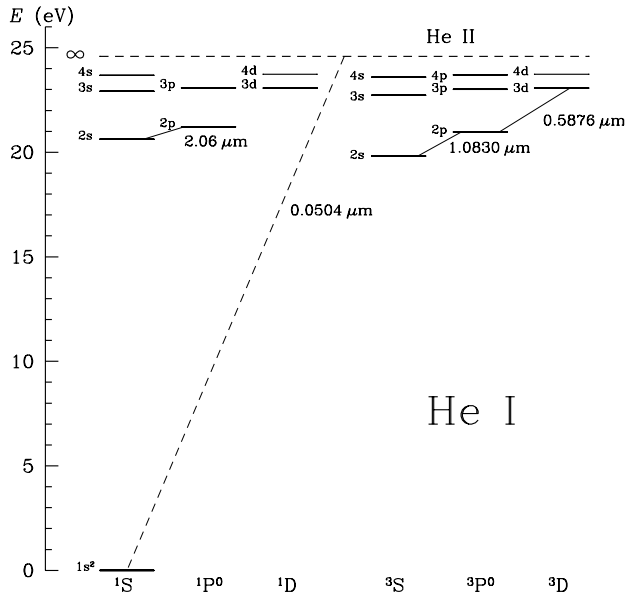

Fig. 3. Energy level diagramme of He I. For clarity, levels for quantum numbers >4 have been omitted. The transitions, which are discussed in the text, i.e. 1.0830 μm and 0.5876 μm of the triplet states and 2.06 μm of the singlets, are marked and the wavelength of He I ionization is shown next to the slanted dashed line (see also Fig. 2).

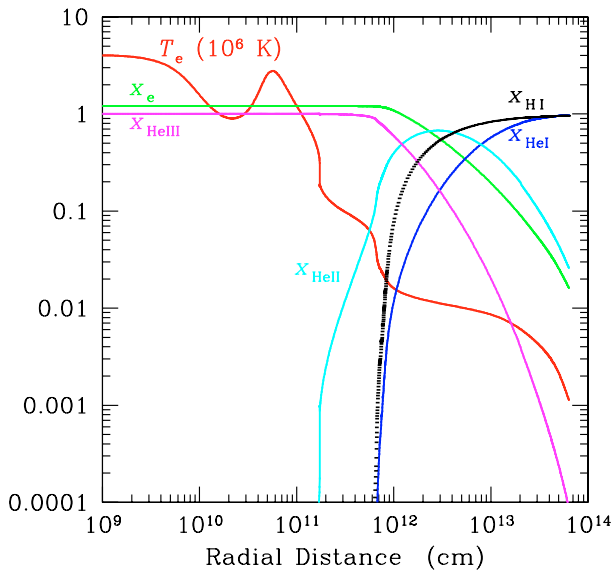

Fig. 4. Helium ionization structure of gas with constant density $n(\mathrm{H}) = 10^5$ cm^{-3}, being illuminated by a 4 MK point source. The run of the temperature T_e (in units of 10^6 K) is shown in red, that of the electron fraction x_e in green. The fractional H I density is shown by the black broken line, whereas those of He I, He II and He III in blue, cyan and magenta, respectively. Tests with the previous version Cloudy 90 gave essentially identical results, except that the temperature structure is smoother. The hump due to "ionization jumps" for a number of species is absent, indicating that this feature does not have any major effect on the results of interest.

observed X-rays are sufficientally energetic to photoionize helium (see Fig. 2) resulting in He 1.0830 emission upon recombination. But is it possible to explain the fact that the observed line intensity ratio He I 1.0830 μm/Pγ 1.0938 μm $\gg 1$? Such inverted ratios are generally not revealed by models of jet shocks (e.g. Hartigan et al. 1987), but have been observed to develop in supernova ejecta (e.g. Meikle et al. 1993; Pozzo et al. 2004).

For the model calculations we used the program Cloudy (version 96 last described by Ferland et al. 1998), which determines the temperature structure for a gas of a certain geometry and density, including the transfer of radiation. For the calculations described here, the shape of the X-ray input spectrum is that of a blackbody (Fig. 2), scaled by the observed X-ray luminosity, i.e. the inner radius is $r_{\rm in} = \sqrt{L_{\rm X}/4\pi\sigma T^4}$. The outer radius of the spherical cloud was initially set by the observed X-ray emission measure and the assumed constant density, i.e. $r_{\rm out} \sim (3\,EM/4\pi)^{1/3} n(\mathrm{H})^{-2/3}$. Solar abundances were assumed for the chemical composition of the gas, hence $n(\mathrm{He})/n(\mathrm{H}) = 0.1$.

The resulting model for $n(\mathrm{H}) = 10^5$ cm^{-3}, which is in fair agreement with the observations, is depicted in Fig. 4. In particular, the ratios He I 1.0830 μm/Pγ 1.0938 μm and He I 1.0830 μm/Pβ 1.2818 μm are 13 and 7, respectively, i.e. both much larger than unity as has been observed (Table 2). According to the model, with e$^-$-collision coefficients from Bray et al. (2000), the excitation of the He I 1.0830 μm line is dominated by collisions, so that in this case, the "10830 recombination line" is not really due to He recombination (compare the $x_{\rm He\,II}$ and $x_{\rm He\,I}$ regions in the figure). For purely thermal broadening, the line would be marginally optically thick, i.e. $\tau = 1.5$ at the center of the line. The flux of the reddened 2.06 μm line (Fig. 3) is predicted not to exceed the 10% level of that in the 1.0830 μm line.

A hint to the nature of the He I excitation is potentially also provided by the He I 0.5876 μm line, originating from the state just above that of the He I 1.0830 μm line (see Fig. 3). The line intensity ratio He I 0.5876 μm/He I 1.0830 μm of the model is 0.3, i.e. the predicted (reddened) He I 0.5876 μm flux is 4×10^{-16} erg cm^{-2} s^{-1}. This is in agreement with the observation by Cohen & Fuller (1985), which resulted in an upper limit, i.e. $F < 6.5 \times 10^{-16}$ erg cm^{-2} s^{-1} (the units in that paper seem erroneous). Given the information provided by Cohen & Fuller (1985), it seems not likely, however, that this measurement actually refers to the location of the X-ray source. In addition, the X-ray emission is known to be variable on short time scales (Favata et al. 2006).

The observed He I 1.0830 μm luminosity (Sect. 2.1.4) is a sizable fraction of the X-ray luminosity and it comes hardly as a surprise that the model falls short with regard to $L_{1.0830\ \mu\rm m}$. This may not be attributable solely to source variability. In principle, an ad hoc increase of the emitting volume could artificially cure this luminosity problem: for instance, shock models would lead to typically much larger cooling lengths (10^{15}–10^{16} cm) than what is indicated in Fig. 4 ($<10^{14}$ cm). The required increase by an order of magnitude seems consistent with the models of X-ray emitting bow shocks of Raga et al. (2002). Also, as suggested by the referee, a jet with a time variability in the ejection velocity could increase the emitting volume (hence the total luminosity). This volume increase is produced when two successive working surfaces collide with each other.

However, such an ad hoc procedure would lack any physical justification. Therefore, rather than trying "to fix" this poor model, one would like to see a proper time-dependent hydrodynamical calculation for the high velocity jets, accounting for the shocks and the cooling in a self-consistent manner. This is also warranted by the various time scales of the steady state photoionization model (e.g., for thermal equilibrium and hydrogen recombination), which are all very much longer than the dynamical time scale of less than one year.

On the observational side, one would like to see concerted efforts of X-ray observations and simultaneous intermediate to high resolution ($R \geq$ a few $\times 10^3$) infrared spectroscopy.

Acknowledgements. The thoughtful comments by the anonymous referee are gratefully acknowledged.

References

Bonito, R., Orlando, S., Peres, G., Favata, F., & Rosner, R. 2004, A&A, 424, L 1
Bray, I., Burgess, A., Fursa, D. V., & Tully, J. A. 2000, A&AS, 146, 481
Cohen, M., & Fuller, G. A. 1985, ApJ, 296, 620
Favata, F., Fridlund, C. V. M., Micela, G., Sciortino, S., & Kaas, A. A. 2002 A&A, 386, 204
Favata, F., Bonito, R., Micela, G., et al. 2006, A&A, 450, L 17
Ferland, G. J., Korista, K. T., Verner, D. A., et al. 1998, PASP, 110, 761
Fridlund, C. V. M., Liseau, R., Djupvik, A. A., et al. 2005, A&A, 436, 983
Giannini, T., Nisini, B., Caratti o Garatti, A., & Lorenzetti, D. 2002, ApJ, 570, L 33
Giannini, T., McCoey, C., Caratti o Garatti, A., et al. 2004, A&A, 419, 999
Giannini, T., Massi, F., Podio, L., et al. 2005, A&A, 433, 941
Grosso, N., Feigelson, E. D., Getman, K. V., et al. 2006, A&A, 448, L 29
Güdel, M., Skinner, S. L., Briggs, K. R., et al. 2005, ApJ, 626, L 53
Hartigan, P., Raymond, J., & Hartmann, L. 1987, ApJ, 316, 323
Hummer, D. G., & Storey, P. J. 1997, MNRAS, 224, 801
Itoh, Y., Kaifu, N., Hayashi, M., et al. 2000, PASJ, 52, 81
Liseau, R., Fridlund, C. V. M., & Larsson, B. 2005, ApJ, 619, 959
McCoey, C., Giannini T., Flower, D. R., & Caratti o Garatti, A. 2004, MNRAS, 353, 813
Meikle, W. P. S., Spyromilio, J., Allen, A. D., Varani, G.-GF., & Cumming, R. J. 1993, MNRAS, 261, 535
Nisini, B., Bacciotti, F., Giannini, T., et al. 2005, A&A, 441, 159
Ostriker, J. P., & McKee, C. F. 1988, Rev. Mod. Phys., 60, 1
Pozzo, M., Meikle, W. P. S., Fassia, A., et al. 2004, MNRAS, 352, 457
Preibisch, T. 2003, A&A, 410, 951
Pravdo, S. H., Feigelson, E. D., Garmire, G., et al. 2001, Nature, 413, 708
Pravdo, S. H., Tsuboi, Y., & Maeda, Y. 2004, ApJ, 605, 259
Quinet, P., Le Dourneuf, M., & Zeippen, C. J. 1996, A&AS, 120, 361
Raga, A. C., Böhm, K.-H., & Cantó, J. 1996, RMxAA, 32, 161
Raga, A. C., Noriega-Crespo, A., & Velázquez, P. F. 2002, ApJ, 576, L 149
Reipurth, B. 1999, A general catalogue of Herbig-Haro objects, 2 edn., `http://casa.colorado.edu/hhcat`
Reipurth, B., & Bally, J. 2001, ARA&A, 39, 403
Rieke, G. H., & Lebofsky, M. J. 1985, ApJ, 288, 618
Takami, M., Chrysostomou, A., Bailey, J., et al. 2002, ApJ, 568, L 53
Tsujimoto, M., Koyama, K., Kobayashi, N., et al. 2004, PASJ, 56, 341
White, G. J., Liseau, R., Men'shchikov, A. B., et al. 2000, A&A, 364, 741
Zirin, H. 1982, ApJ, 260, 655